45th AIAA Aerospace Sciences Meeting and Exhibit
8 - 11 January 2007, Reno, Nevada

AIAA 2007-440

SMALL-APERTURE PHASED ARRAY STUDY OF NOISE FROM COAXIAL JETS

Dimitri Papamoschou*
University of California, Irvine, California 92697-3975

The noise source distribution of coaxial jets at variable velocity ratio is investigated with a small-aperture microphone phased array. The array design enables discrimination between noise emitted by large-scale turbulence (direction of peak emission) and noise emitted by fine-scale turbulence (broadside direction). For zero velocity ratio (single-stream jet), the near field emits strong high-frequency noise. Increasing the velocity ratio suppresses the near-field noise by as much a 9 decibels and extends downstream the location of the peak noise, which increases moderately. The acoustic trends with velocity ratio are similar for the two types of noise sources, although the increase in peak noise is more pronounced for the large-scale noise.

Nomenclature

D	=	nozzle diameter
f	=	cyclic frequency
F	=	static thrust
G_{mn}	=	cross spectrum matrix
$\ell_m(x)$	=	distance of microphone m from focus point x
m_0	=	number of microphones
M	=	jet Mach number
R	=	array radius
$s(x,t)$	=	delay-and-sum array output
Sr	=	Strouhal number = fD_p/U_p
t	=	time
U	=	jet velocity
w_m	=	weight for microphone m
$\bar{w}_m$	=	dimensionless weight for microphone m
x	=	axial coordinate
ϵ_m	=	weighted steering vector
λ	=	wavelength
$\Phi(x,\omega)$	=	array power spectrum (Pa^2/Hz)
$\Phi_{\text{SPL}}(x,f)$	=	lossless array sound pressure level spectrum (dB/Hz)
τ_m	=	time delay for microphone m
ω	=	radian frequency = $2\pi f$

Subscripts

a	=	average among microphones
p	=	primary
s	=	secondary
wa	=	weighted average among microphones

*Professor, Associate Fellow AIAA

I. Introduction

Noise from coaxial jets has strong relevance to aeroacoustics because the majority of civilian turbofan engines have a coaxial exhaust. Early works on coaxial jets were motivated mainly by applications in combustion and aircraft propulsion. Forstall and Shapiro[1] conducted an experimental investigation on mass and momentum transfer between the two streams of a coflowing jet with very large secondary flows. They determined that the velocity ratio of the primary to secondary stream is the principal variable determining the shape of the mixing region. An empirical relation for the length of the primary potential core was proposed. Other works in subsonic, axisymmetric, turbulent coaxial jets have studied the near-field region at various velocity ratios. Ko and Kwan,[2] Champagne and Wygnanski,[3] and Durao and Whitelaw[4] investigated the development of the flow field and its approach to a self-preserving state. These studies concluded that the instability and flow development depend on the velocity and density ratios across the shear layers. Williams et al.[5] investigated the flow structure and acoustics of cold subsonic coaxial jets and suggested a method for predicting the noise attenuation when the jet is surrounded by an annular flow of variable velocity. Murakami and Papamoschou[6] conducted a parametric study of the mean flow field of coaxial jets and noted the substantial elongation of the primary potential core with addition of a secondary flow.

A number of studies have focused on the acoustic benefit of using a coaxial jet versus a single jet.[7–10] Tanna[8] concluded that subsonic coaxial jets with normal velocity profile are noisier, in terms of overall sound pressure level, when compared to a single equivalent jet (SEJ) with the same thrust, mass flow rate, and exit area. Zaman and Dahl[10] used the criterion of equal enthaply (instead of equal area) to define the SEJ and arrived basically at the same conclusions as Tanna. On the other hand, experiments on supersonic coaxial jets by Papamoschou[11] showed that the coaxial jet is slightly quieter than the SEJ. It appears therefore that the acoustic differences between a coaxial jet and its SEJ depend on the flow parameters.

For jets representing modern high-bypass engines, there is little doubt that the SEJ is quieter than the coaxial jet. However, the uniformly-mixed SEJ is an idealization. In practice, the exhaust is non-uniform and the mixer creates its own noise and weight penalties. For these and other practical considerations the majority of high-bypass engines are of the unmixed (separate-flow) type. This is the reason coaxial jets remain the focus of intense activity to understand their fluid dynamics and acoustics, and to suppress their noise.

The present work is motivated by the ability of the secondary flow in a coaxial jet to suppress noise from the primary flow. Fisher et al.[12] studied coaxial jets with normal velocity profile and suggested that, in the initial region where a secondary potential core exists, the primary shear layer (between the primary and secondary flows) makes a negligible contribution to sound emission. Papamoschou[13] extended this concept to a secondary core defined by the inflection points of the velocity profile and showed that the convective Mach number of eddies in the initial region has very low value. The ability of the secondary flow to silence the primary shear layer is the foundation of noise-reduction concepts that extend the secondary core (via offset nozzles or deflectors) to cover a greater portion of the primary shear layer that emits downward noise.[11,13–15]

The advent of noise-source location techniques, such as microphone phased arrays, provides an opportunity for a more detailed investigation of the changes in acoustics as a function of velocity ratio in coaxial jets. Of interest are the silencing of the initial region and the downstream extension of noise sources due to the elongation of the primary potential core. This study treats the jet as a line source, shown in Fig.1, and employs traditional beamforming techniques to generate noise source maps. The microphone array has narrow aperture to distinguish among the different types of noise sources present in the jet.[16] This paper provides only a brief overview of the noise source location technique for the narrow-aperture array. Further details can be found in Papamoschou and Dadvar.[17]

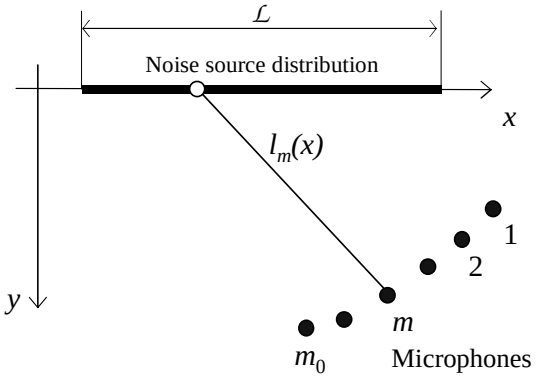

Fig.1 Linear distribution of noise sources and microphone array.

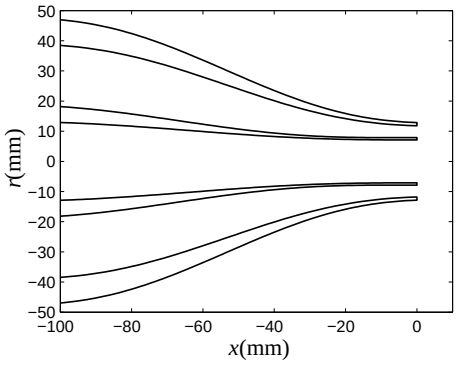

Fig. 2 Nozzle coordinates.

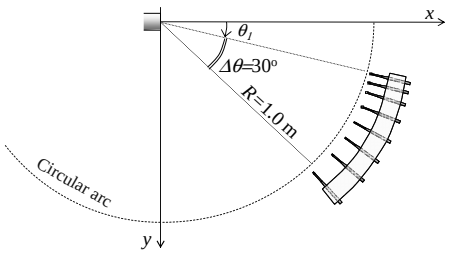

Fig. 3 Geometry of microphone phased array.

II. Experimental Setup

A. Flow facility

Experiments were conducted in U.C. Irvine's Jet Aeroacoustics Facility, described in earlier publications.[18] A coaxial dual-stream nozzle with exit diameters D_p=14.2 mm and D_s =23.6 mm was employed. The nozzle coordinates are plotted in Fig.2. Air at room temperature was supplied to the primary and secondary streams. The Mach number of the primary stream was fixed at $M_p = 0.9$ and the secondary Mach number M_s was varied from 0 to 0.9 in increments of 0.15. Table 1 lists the flow conditions. Cases are labeled according to their velocity ratio (i.e., R036 means U_s/U_p=0.356). The Reynolds number of the primary jet was 3.2×10^5.

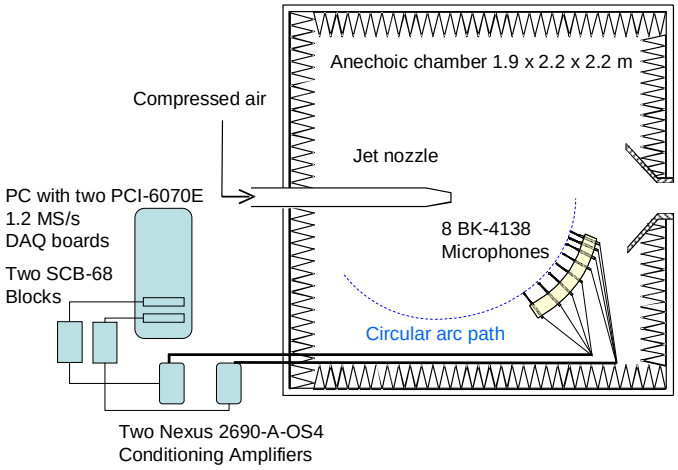

Fig.4 Primary components of microphone array system.

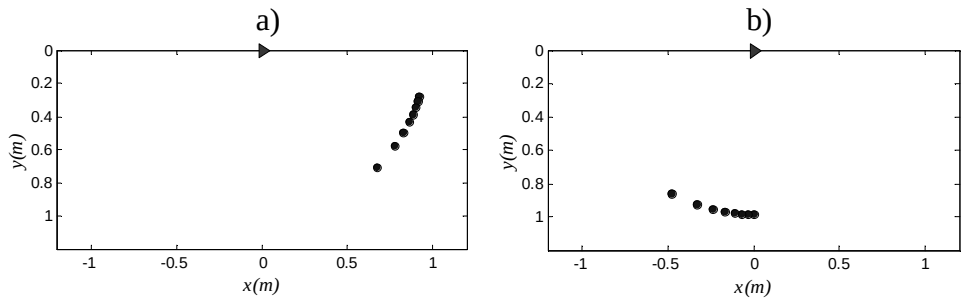

Fig.5 Two positions of array: a) $\theta_{wa} = 30^o$; b) $\theta_{wa} = 99^o$. Triangles indicate nozzle exit.

Table 1 Flow Conditions ($M_p = 0.90$, U_p=285 m/s)

Case	M_s	U_s (m/s)	U_s/U_p	F(N)
R000	0.00	0.0	0.000	18.5
R018	0.15	51	0.179	19.1
R036	0.30	101	0.356	21.6
R053	0.45	151	0.528	25.4
R069	0.60	198	0.694	31.0
R085	0.75	243	0.852	37.7
R100	0.90	285	1.000	46.1

B. Microphone Phased Array

The microphone phased array consists of eight 3.2-mm condenser microphones (Brüel & Kjær Model 4138) arranged on a circular arc centered at the vicinity of the nozzle exit. Figure 3 shows the array geometry. The polar aperture of the array for this experiment was 30° and the array radius was 1 m. The angular spacing of the microphones was logarithmic, starting from 2° for microphones 1 and 2 and ending with 10° for microphones 7 and 8. Uneven microphone spacing was used to mitigate the effects of spatial aliasing. The entire array structure is rotated around its center to place the array at the desired observation angle. Positioning of the array was done remotely using a stepper motor. An electronic inclinometer displayed the position of the first microphone. The distances between the centers of the microphone grids were measured with accuracy of 0.1 mm using a digital caliper. A geometric calibration procedure provided the position of

each mirophone relative to the nozzle exit with accuracy of 2 mm.

The arrangement of the microphones inside the anechoic chamber, and the principal electronic components, are shown in Fig. 4. The microphones were connected, in groups of four, to two amplifier/signal conditioners (Brüel & Kjær Nexus 2690-A-OS4) with low-pass filter set at 300 Hz and high-pass filter set at 100 kHz. The four-channel output of each amplifier was sampled at 250 kHz per channel by a multi-function data acquisition board (National Instruments PCI-6070E). Two such boards, one for each amplifier, were installed in a Pentium 4 personal computer. National Instruments LabView software was used to acquire the signals. For each jet configuration the array was placed at four positions, the polar angle of the first microphone taking the values of 15, 40, 65, and 90 deg.

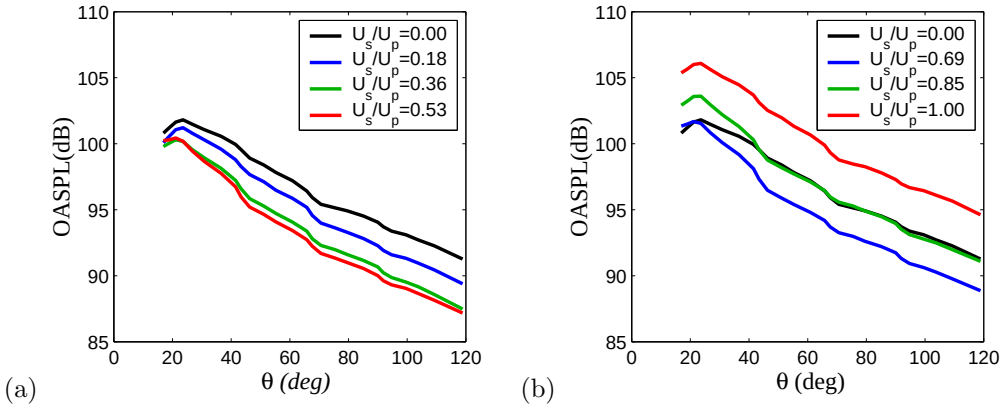

Fig. 6 Overall sound pressure level versus polar angle (a) $U_s/U_p < 0.69$**; (b)** $U_s/U_p \geq 0.69$**.**

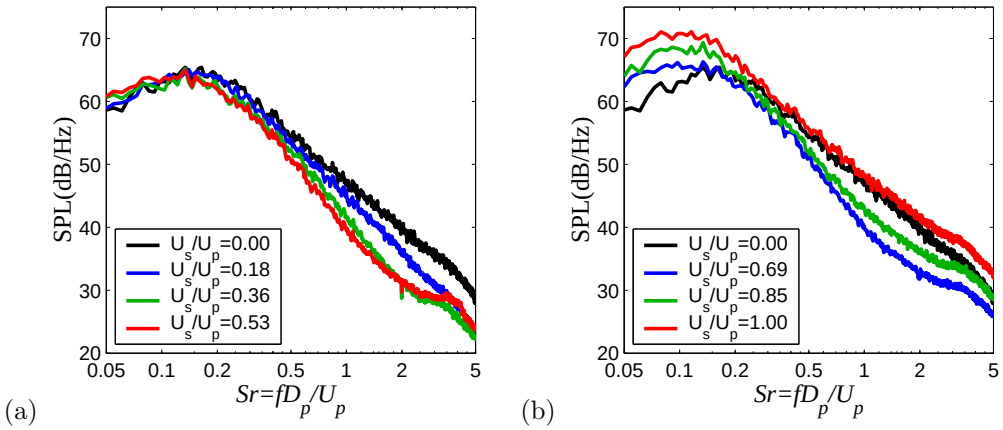

Fig. 7 Spectra in the direction of peak emission. (a) $U_s/U_p < 0.69$**; (b)** $U_s/U_p \geq 0.69$

C. Beamforming

Referring to Fig. 1, beamforming uses the traditional delay-and-sum method,

$$s(t) = \sum_{m=1}^{m_0} w_m p_m(t + \tau_m) \tag{1}$$

where $p_m(t)$ is the pressure fluctuation measured by microphone m, w_m are weights, and

$$\tau_m = \frac{\ell_m(x)}{a} \tag{2}$$

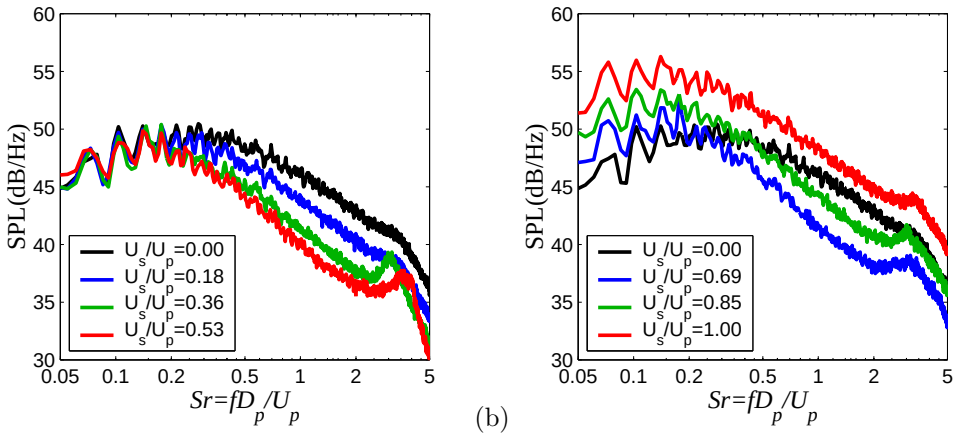

Fig. 8 Spectra in the 90-deg direction. (a) $U_s/U_p < 0.69$**; (b)** $U_s/U_p \geq 0.69$**.**

is the time delay for sound to propagate from the steering point x to microphone m. The power spectrum of $s(t)$ is

$$\Phi(x,\omega) = \sum_{m=1}^{m_0}\sum_{n=1}^{m_0} w_m w_n e^{i\omega(\tau_m-\tau_n)} < P_m(\omega)P_n^*(\omega) > \tag{3}$$

where

$$P_m(\omega) \;=\; \int_{-\infty}^{\infty} p_m(t)e^{-i\omega t}dt \tag{4}$$

and <> denotes time-averaging. Defining the cross-spectrum matrix as

$$G_{mn} \;\equiv < P_m(\omega)P_n^*(\omega) > \tag{5}$$

we have

$$\Phi(x,\omega) = \sum_{m=1}^{m_0}\sum_{n=1}^{m_0} w_m w_n e^{i\omega(\tau_m-\tau_n)} G_{mn} \tag{6}$$

or

$$\Phi(x,\omega) \;=\; \epsilon \mathbf{G} \epsilon^T \tag{7}$$

where

$$\epsilon_m(x,\omega) \;=\; w_m(x,\omega)e^{i\omega\tau_m(x)} \tag{8}$$

is the weighted steering vector and superscript T denotes its complex transpose. Eq. 7 formed the basis for the computation of the array power spectrum from the microphone pressure traces.

It is important to realize that the array output given by Eq. 7 is a convolution between the source distribution (assumed incoherent) and the point spread function. A primary consideration in selecting the form of the weights is that the area under the main lobe of the point spread function remain substantially constant with focus point x. This prevents artificial distortions of the apparent source distribution due to axial variation of the point spread function. Earlier research has shown that this can be accomplished by making the weights inversely proportional to the transverse distance of the microphone from the line source, i.e., $w_m \sim 1/y_m$. To maintain constant beam width with frequency, the weights include the frequency dependence $w_m \sim \sqrt{Sr}$. The resulting form for the weights is

$$w_m \;= \frac{R}{\sum_1^{m_0} \bar{w}_m}\; \bar{w}_m \frac{y_m}{y_a}\sqrt{Sr} \tag{9}$$

The non-dimensional weights $\bar{w}_m$ were selected so that the beamwidth in the middle of the region of interest (around x/D_p=10) was roughly the same for the two array positions used for noise source location. Table 1

provides the microphone angles and non-dimensional weights for each array position. The array observation polar angle is defined as the weighted average of the microphone polar angles

$$\theta_{\text{wa}} = \frac{\sum_1^{m_0} w_m \theta_m}{\sum_1^{m_0} w_m} \tag{10}$$

Computation of the cross spectrum matrix, Eq. 5, involved the following steps. Each microphone signal consisted of $N_s = 2^{18} = 262144$ samples acquired at a sampling rate $F_s = 250$ kHz. The maximum resolvable (Nyquist) frequency was $F_s/2 = 125$ kHz, although the high-pass filter was set a little lower at f=100 kHz. The size of the Fast Fourier Transform was $N_{\text{FFT}} = 2024$ yielding a frequency resolution of 122 Hz. Each signal was divided into $K = 64$ blocks of 4096 samples each, and the data within each block was windowed using a Hamming window. The cross-spectrum matrix G^k_{mn} for block k was computed using Fortran routines for autospectra and crossspectra. The total cross-spectrum matrix was obtained from

$$G_{mn}(f) = \frac{1}{KW_h} \sum_{k=1}^{K} G^k_{mn}(f) \tag{11}$$

where W_h is a weighting constant for the Hamming window.

To present the array power spectrum in the form of a lossless sound pressure level spectrum (units of decibels), the following procedure was used:

$$\Phi_{\text{SPL}}(x, f) = 10 \log_{10} [\Phi(x, f)] + 93.98 - C_{\text{fr}}(f) - C_{\text{ff}}(f) + \alpha(f)\ell_a(x) \tag{12}$$

The constant 93.98 comes from the normalization of the pressure by the reference pressure of 20 μPa, that is, $-20 \log_{10}(20 \times 10^{-6}) = 93.98$. C_{fr} and C_{ff} are the corrections for the actuator response and free-field response, respectively; they are based on data provided by the manufacturer of the microphone and are practically the same for all the microphones. α is the atmospheric absorption coefficient (dB/m), computed using the formulas proposed by Bass et al.[22] for the measured values of relative humidity and temperature of the ambient air. The absorption correction is based on the average distance $\ell_a(x)$ of the microphones from the focus point. The last step in the processing involves smoothing of the array power spectrum in frequency, using a Savitsky-Golay filter, to remove spurious wiggles that are unrelated to jet noise physics.

The source-location aspects of this study focus on data obtained at two array observation angles, as defined by Eq. 10: $\theta_{\text{wa}} = 30°$ and $\theta_{\text{wa}} = 99°$. They correspond to noise generated by large-scale and fine-scale turbulence, respectively.[16] The placement of the microphones for each observation angle is plotted in Fig. 5.

Table 1 Microphone Array Parameters

$\theta_{\text{wa}} = 30°$		$\theta_{\text{wa}} = 99°$	
θ	$\bar{w}$	θ	$\bar{w}$
17.1	1.00	76.8	0.56
19.0	1.00	78.6	0.67
21.3	1.00	80.8	0.80
23.9	1.00	83.3	0.92
27.1	1.00	86.4	1.00
31.3	1.00	90.4	0.95
37.0	1.00	95.0	0.57
45.8	1.00	105.5	0.17

III. Results

A. Acoustics

The measurements of far-field acoustics are examined first. Figure 6 plots the directivity of the overall sound pressure level (OASPL) for different velocity ratios. It is important to realize that, as the velocity ratio rises,

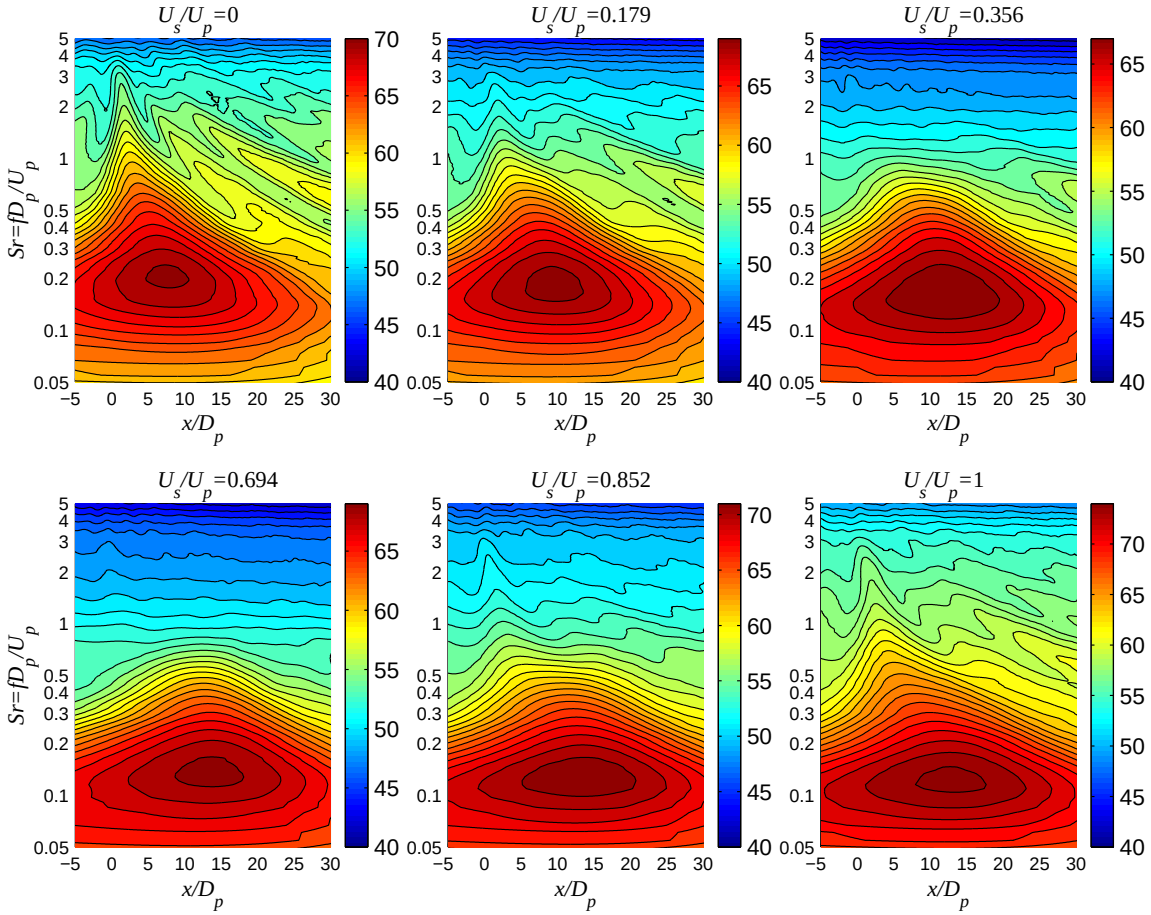

Fig.9 Isocontours of $\Phi_{\mathbf{SPL}}$ in the direction $\theta_{\mathbf{wa}} = 30^o$ and for various velocity ratios.

the thrust of the jet increases. The OASPL data, and the spectra shown later, are not adjusted for constant thrust. With increasing U_s/U_p, the OASPL first decreases and then increases. The minimum OASPL occurs at U_s/U_p=0.53. For $U_s/U_p = 1.0$, where the jet becomes essentially a single jet issuing from a larger nozzle diameter, the OASPL is uniformly 4 dB above the OASPL of the single jet. This is exactly the increase one would predict from geometric thrust scaling arguments:

$$\Delta\text{OASPL} \;=\; 10\log_{10}\left(\frac{F_{R100}}{F_{R000}}\right) \;=\; 10\log_{10}\left(\frac{D_s^2 - D_p^2}{D_p^2}\right) = 4.0 \text{ dB}$$

The lossless narrowband SPL spectra in the direction of peak emission (θ = 25 deg.) are shown in Fig. 7. The overall trend with velocity ratio is the same as with the OASPL, i.e., a decrease followed by an increase in spectral levels as U_s/U_p increases from zero. For $0 < U_s/U_p \leq 0.53$, the spectrum decreases for Strouhal numbers greater than the peak value of $S_r \approx 0.15$, while the low-frequency end of the spectrum stays practically unchanged. Increasing the velocity ratio above U_s/U_p=0.53 increases the high-frequency part of the spectrum (relative to the minimum value attained at U_s/U_p=0.53) as well as the low-frequency end (relative to the single jet). For U_s/U_p=1, the entire spectrum is above that of the single jet. Had the U_s/U_p=1 spectrum been plotted against the Strouhal number based D_s, it would have been uniformly higher than the spectrum for U_s/U_p=0 by about 4 dB. The trends observed for the spectra in the direction of peak emission translate well for the spectra in the 90-deg direction plotted in Fig.8. Small spectral bumps around $Sr = 3$ are probably due to vortex shedding from the blunt lip of the inner nozzle (the lip thickness was 0.8 mm); they do not affect the general conclusions of this study. The aforementioned trends in OASPL and spectra agree with those found by Zaman and Dahl[10] in coaxial jets with similar Mach numbers.

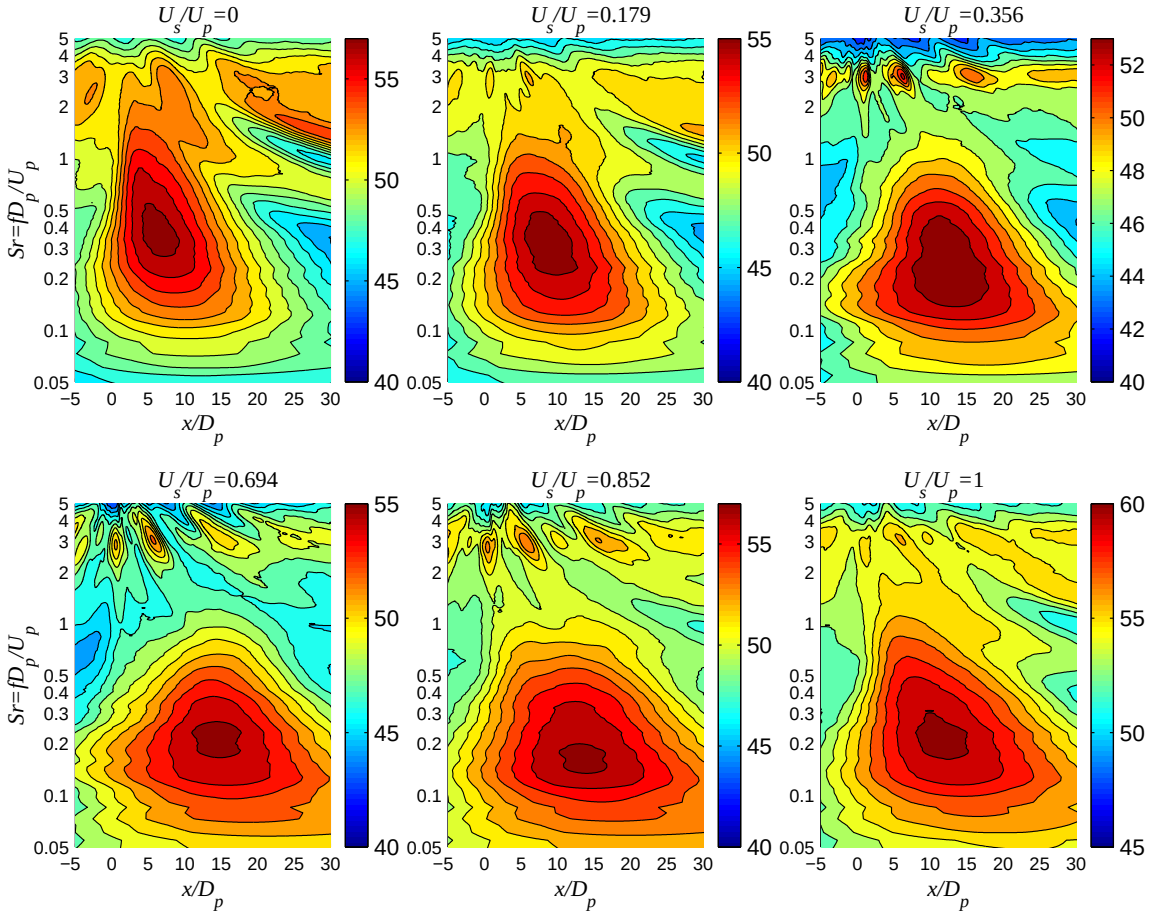

Fig.10 Isocontours of Φ_{SPL} in the direction $\theta_{\mathrm{wa}} = 99^o$ and for various velocity ratios.

B. Source Localization

We now discuss results arising from the beamforming procedure of Section II.C. Figure 9 presents isocontours of $\Phi_{\mathrm{SPL}}(x/D_p, Sr)$ for $\theta_{\mathrm{wa}} = 30°$ and for six of the velocity ratios investigated. For the single jet ($U_s/U_p = 0$), the maximum level is located at $x/D_p = 7.5$ and $Sr = 0.2$. The axial location of the maximum level is close to the end of the potential core, as determined by mean velocity surveys of this flow (see for example Fig. 12 of Ref. 16). We observe a high-frequency "spike" as $x \to 0$, indicating that the near-field region emits strong high-frequency noise. Introduction of a slower secondary flow reduces the spike and for $0.356 \leq U_s/U_p \leq 0.694$ the spike disappears. It reappears when the velocity ratio becomes large. The elimination of the high-frequency spike indicates that the secondary flow suppresses near-field noise. The other important trend in Fig.9 is that, with increasing velocity ratio, the peak noise level moves downstream, reflecting the elongation of the primary potential core with addition of the secondary flow. For $U_s/U_p = 1.00$, where the jet essentially becomes a single jet issuing from a larger nozzle, we recover the acoustics of the single (R000) jet. The contours for $U_s/U_p = 1.00$ would match those for $U_s/U_p = 0.00$ if the axial distance and frequency were non-dimensionalized with D_s instead of D_p.

The noise source maps in the direction $\theta_{\mathrm{wa}} = 99°$, shown in Fig. 10, look significantly different from those at $\theta_{\mathrm{wa}} = 30°$ owing to the flatter spectrum in this direction. However, the trends with velocity ratio are fundamentally the same as for $\theta_{\mathrm{wa}} = 30°$: the secondary flow suppresses high-frequency noise near the nozzle exit and extends downstream the location of peak noise.

A clearer picture of the effect of the secondary flow on the noise source distribution is gained by computing a differential noise map, that is, the difference between a given configuration and the single jet. The differential

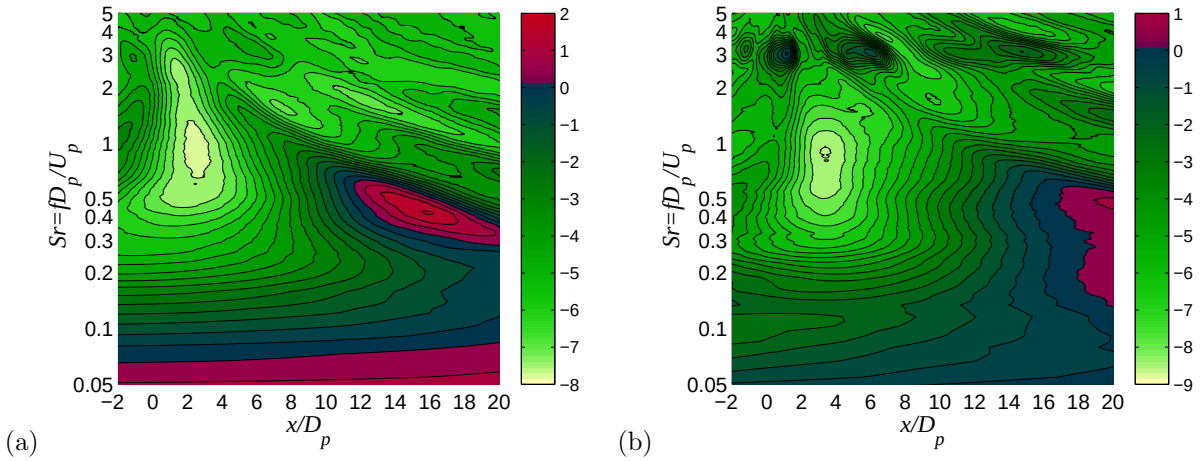

Fig. 11 Differential noise source maps showing the difference between $U_s/U_p = 0.356$ and $U_s/U_p = 0$. (a) $\theta_{\mathbf{wa}} = 30^o$; (b) $\theta_{\mathbf{wa}} = 99^o$.

maps for U_s/U_p=0.356 are shown in Fig. 11 for array angles $\theta_{\text{wa}} = 30°$ and 99°. Green-based colors indicate noise suppression and red-based colors indicate noise increase. In the first 2-3 jet diameters the noise sources are suppressed significantly, by as much 9 dB at $S_r \approx 1$. For the large-scale noise ($\theta_{\text{wa}} = 30°$) there is a moderate increase in low-frequency sound at $x/D_p \sim 15$ of about 2 dB. The same trend is also observed for the fine-scale noise ($\theta_{\text{wa}} = 99°$) but it is less pronounced and occurs at $x/D_p \sim 20$.

The elongation of the noise source region with addition of the secondary flow is further evident in Figure 12 which plots the location of the peak noise on the $x/D_p - Sr$ plane for $\theta_{\text{wa}} = 30°$ than at $\theta_{\text{wa}} = 99°$. Similar trends are observed for both array angles. For the single jet, the peak noise source location is similar to that measured in past studies of subsonic jets.[19,20]

The effect of velocity ratio on the space-frequency location of the global peak of the noise source distribution is shown in Figs. 13 and 14. The axial location of the peak versus velocity ratio, plotted in Fig. 13, is roughly the same for the two array observation angles. As U_s/U_p increases from 0 to 0.56, the axial location of the peak moves from $x/D_p = 7$ to $x/D_p = 14$. Further increase of U_s/U_p leads to a slight retraction of the peak to $x/D_p = 12$ at U_s/U_p=1. The latter corresponds to x/D_s=7, that is, the same non-dimensional distance as for the single jet. Figure 14 shows that the Strouhal number of the peak noise, Sr_{peak}, decreases with increasing velocity ratio. For $\theta_{\text{wa}} = 30°$, Sr_{peak} declines from 0.21 at $U_s/U_p = 0$ to 0.12 at $U_s/U_p = 1$. The corresponding decline for $\theta_{\text{wa}} = 99°$ is 0.40 to 0.22. At $U_s/U_p = 1$ the Strouhal numbers based on D_s are fD_s/U_p=0.20 and 0.37 for $\theta_{\text{wa}} = 30°$ and $\theta_{\text{wa}} = 99°$, respectively, thus coming close to the values of the single (R000) jet.

IV. Concluding Remarks

The noise source distribution of coaxial jets at variable velocity ratio is investigated with a small-aperture microphone phased array. The array design enables discrimination between noise emitted by large-scale turbulence (direction of peak emission) and noise emitted by fine-scale turbulence (broadside direction). For zero velocity ratio (single-stream jet), the near field emits strong high-frequency noise. Increasing the velocity ratio suppresses the near-field noise by as much a 9 decibels and extends downstream the location of the peak noise, which increases moderately. The suppression of near-field noise is consistent with the reduced shear and reduced convective Mach number elucidated in earlier studies[12,13] The acoustic trends with velocity ratio are similar for the two types of noise sources, although the increase in peak noise is more pronounced for large-scale noise. The results indicate that the coaxial jet has a noise source distribution fundamentally different from that of a single-stream jet.

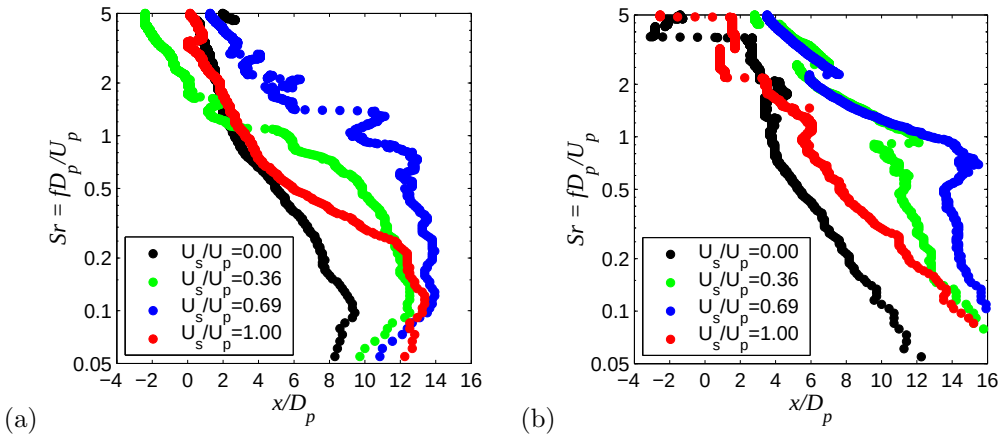

Fig. 12 Locus of peak noise on $x/D - Sr$ diagram for various velocity ratios. (a) $\theta_{wa} = 30^o$; (b) $\theta_{wa} = 99^o$.

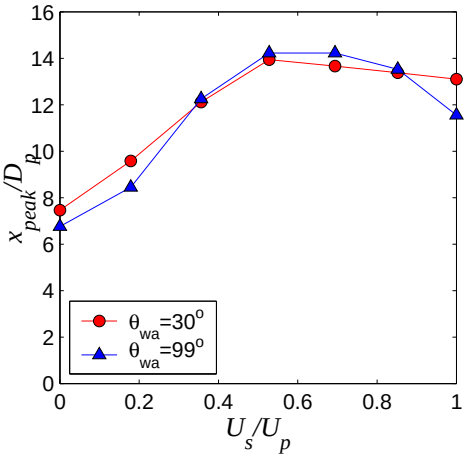

Fig.13 Axial location of peak noise.

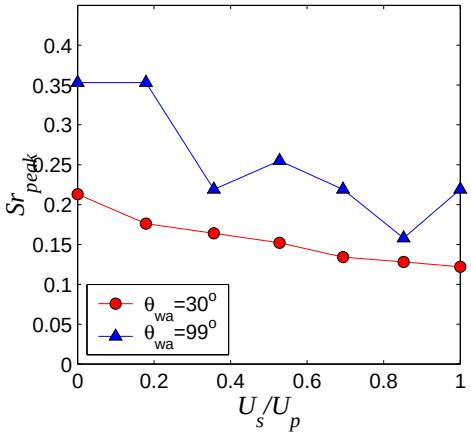

Fig.14 Strouhal number of peak noise.

References

[1] Forstall, W. Jr., and Shapiro, A.H., "Momentum and Mass Transfer in Coaxial Gas Jets," *Journal of Applied Mechanics*, Vol. 10, 1950, pp. 399-408.

[2] Ko, N.W.M., and Kwan, A.S.H., "The Initial Region of Subsonic Coaxial jets," *Journal of Fluid Mechanics*, Vol. 73, Part 2, 1976, pp. 305-332.

[3] Champagne, F.H., and Wygnanski, I.J., "An Experimental Investigation of Coaxial Turbulent Jets," *International Journal of Heat and Mass Transfer*, Vol. 14, 1971, pp. 1445-1464.

[4] Durao, D., and Whitelaw, J.H., "Turbulent Mixing in the Developing Region of Coaxial Jets," *Journal of Fluids Engineering*, Vol. 95, No. 3, 1973, pp. 467-473.

[5] Williams, T.J., Ali, M.R.M.H., and Anderson, J.S., "Noise and Flow Characteristics of Coaxial Jets," *Journal of Mechanical Engineering Science*, Vol. 11, No. 2, 1969, pp. 133-142.

[6] Murakami, E., and Papamoschou, D. "Mean Flow Development in Dual-Stream Compressible Jets," AIAA Journal, Vol. 40, No.6, 2002, pp. 1131-1138.

[7] Dahlen, H.W., "Some Experiments on the Noise Emission from Coaxial Jets," *1st International Symposium on Air Breathing Engines*, 1972.

[8] Tanna, H.K., "Coannular Jets- are they really quiet and why?," *Journal of Sound and Vibration*, Vol. 72, 1980, pp. 97-118.

[9] Tanna, H.K., and Morris, P.J., "The Noise from Normal-Velocity-Profile Coannular Jets," *Journal of Sound and Vibration*, Vol. 98, 1985, pp. 213-234.

[10] Zaman, K.B.M.Q., and Dahl, M.D., "Noise and Spreading of a Subsonic Coannular Jet – Comparison with Single Equivalent Jet," AIAA-2005-0210, Jan. 2005.

[11] Papamoschou, D., "Engine Cycle and Exhaust Configurations for Quiet Supersonic Propulsion, " AIAA Journal of Propulsion and Power, Vol.20, No.2, 2004, pp. 255-262.

[12] Fisher, M.J., Preston, G.A., and Bryce, W.D. "A Modelling of the Noise from Simple Coaxial Jets, Part 1: With Unheated Primary Flow," *Journal of Sound and Vibration* Vol. 209, No. 3, 1998, pp. 385-403.

[13] Papamoschou, D., "New Method for Jet Noise Suppression in Turbofan Engines," AIAA Journal, Vol. 42, No.11, 2004, pp. 2245-2253.

[14] Henderson, B., Norum, T., and Bridges, J., "An MDOE Assessment of Nozzle Vanes for High Bypass Ratio Jet Noise Reduction," AIAA-2006-2543, May 2006.

[15] Zaman, K.B.M.Q., and Papamoschou, D. "Effect of a Wedge on Coannular Jet Noise," AIAA-2006-0007, Jan. 2006.

[16] Tam, C.K.W., Golebiowski, M., and Seiner, J.M., "On the Two Components of Turbulent Mixing Noise from Supersonic Jets," AIAA Paper 96-1716, May 1996.

[17] Papamoschou, D., and Dadvar, A., "Localization of Mulitple Types of Jet Noise Sources," AIAA-2006-2644, May 2006.

[18] Papamoschou, D., and Debiasi, M., "Directional Suppression of Noise from a High-Speed Jet," *AIAA Journal*, Vol. 39, No. 3, 2001, pp. 380-387.

[19] Narayanan, S., Barber, T.J., and Polak, D.R., "High Subsonic Jet Experiments: Turbulence and Noise Generation Studies," *AIAA Journal*, Vol. 40, No. 3, 2002, pp. 430-437.

[20] Lee, S.S., and Bridges, J., "Phased-Array Measurements of Single Flow Hot Jets," AIAA-2005-2842, May 2005.

[21] Savitzky, A., and Golay, M.J.E., "Smoothing and Differentiation of Data by Simplified Least Squares Procedures," *Analytical Chemistry*, Vol. 36, No.8, 1964, pp. 1627.

[22] Bass, H.E., Sutherland, L.C., Blackstock, D.T., and Hester, D.M., "Atmospheric Absorption of Sound: Further Developments, " *Journal of the Acoustical Society of America,* Vol. 97, No. 1, 1995, pp. 680-683.